Heavy-Ion Real Potentials for Collisions of Identical Nuclei *

T. Morović ** and W. Greiner

Institut für Theoretische Physik der Universität Frankfurt am Main, Germany

(Z. Naturforsch. **31 a**, 327–343 [1976]; received January 26, 1976)

An improved two-center model has been used to describe the elastic scattering potentials for the collision of identical nuclei. The macroscopic-microscopic approach includes liquid drop (LD) deformation energies, shell corrections and pairing energy corrections. As basis for the microscopic part a two-center shell model has been used with a Hamiltonian including a Thomas-type spin-orbit potential and an l^2 correction term. The model is applied to the sudden and adiabatic type of scattering process, including a compression energy term in the LD part for the former case. Results are given as potential energy surfaces for the adiabatic scattering process and potential energy curves for the sudden scattering process.

1. Introduction

During the last years theoretical work on heavy ion reactions has become more and more interesting as facilities for mutual scattering of heavier and heavier nuclei with increasing energies are becoming available. During such a collision many reactions occur. In this paper we deal with the elastic scattering of identical particles and investigate the real part of the nucleus-nucleus potentials. The investigation of these potentials may illuminate the connection between nuclear fusion and nuclear fission as well as the problem of the existence of nuclear molecules.

Experimental data on elastic scattering (excitation functions, angular distributions) can be reproduced by optical potentials [1]. Such potentials contain no theoretical interpretation and are not unique, so that they represent merely a kind of parametrization of the experimental data. It therefore is of great physical interest to derive optical potentials from more basic knowledge about the nuclear structure. To that end phenomenological collective models [2, 3] as well as microscopic models [4] have been developed.

From the theory of fission it is well known that neither the pure microscopic (shell) nor the pure macroscopic (liquid drop) model describes the potential properly. The best description of fission has been achieved by a hybrid approach, also known as a shell correction method, developed by Strutinsky [5].

* This work was supported by the Bundesministerium für Forschung und Technologie, and by the Gesellschaft für Schwerionenforschung (GSI).

** Present address: Gesamthochschule Kassel, Germany, OE Naturwissenschaften und Mathematik — Arbeitsgruppe Theoretische Physik.

It was a quite natural step to use this model for the construction of real parts of optical nucleus-nucleus potentials. Here we use the deformation parameters of the compound system [6] rather than the relative distance of the two colliding nuclei. This description has already been used [4, 7, 8], but the macroscopic part of the model was too rough, so that the Coulomb-barriers were too high and the binding energy differences between the ground state of the colliding nuclei and the compound system were difficult to reproduce.

In this work an improved parametrization of the macroscopic part of the model has been developed (Section 2). Also an improved two-center single particle potential for the shell correction calculations is used. The prescription that the liquid drop (LD) surface should coincide with the nuclear equipotential surface which contains the nuclear volume, yields the connection to the single particle model which is then described in Section 3. Our systematic study of the sudden type potentials (connected with the appearance of nuclear compression) shows that even in the scattering of very heavy ions nuclear molecules may be observed. We also investigate numerous potential energy surfaces (PES) of the adiabatic type. The sudden and adiabatic potentials serve as limiting cases: For actual reactions the potentials are expected to be between the two, possibly closer to the latter one. The construction of the potentials and, finally, the results of our study on the sudden and adiabatic type scattering potentials are presented in Sects. 4 and 5. Section 6 contains the conclusions.

Throughout the paper we make use of the rotational symmetry of the potential as well as of the reflexion symmetry with respect to the middle plane.

2. Macroscopic Part of the Model

As mentioned in Sect. 1 we are going to use the deformation parameters of the compound nucleus for the construction of the potential rather than the relative distance of the colliding nuclei. As usual, we let the surface of the liquid drop shape coincide with that equipotential surface V_0 of the two-center shell model which contains the nuclear volume.

2.1. Liquid Drop Deformation Energies for the Adiabatic Processes

We write the generating function of the shapes in cylindrical coordinates as

$$\varrho(z', \beta, h, f_0) = \frac{1}{\beta}\left[b^2 - f_0 z'^2 (1 + c z' + d z'^2)\right]^{1/2} \tag{1}$$

where b, c and d still depend on V_0, z_0, β, h and f_0. The coordinate z' is defined as

$$z' = \begin{cases} z - z_0 & \text{if } z \geqq 0, \\ z + z_0 & \text{if } z < 0 \end{cases} \tag{2}$$

where $\pm z_0\,(z_0 \geqq 0)$ denote the position of the centers of the shell model potential.

The deformation parameter β describes the (equal) elliptical deformation of each of the fragments, i.e. the ratio of the figure axes. For $0 < \beta < 1$ one has the oblate and for $\beta > 1$ the prolate deformation (Fig. 1, lower part). The case $\beta = 1$ describes spheres. The pure spheriodal form (for the compound nucleus) is given by Eq. (1) for $z_0 = c = d = 0$, $f_0 = 1$. The constriction deformation parameter h is described by the ratio of the shell model potential (15) at the origin $V(0, 0)$ and the surface potential V_0, $h = V(0, 0)/V_0$ (Fig. 1, upper part) and has the range $0 \leqq h < \infty$. It can be easily seen that the touching configuration is characterized by $h = 1$ *.

In the adiabatic case we have no compression and the figure axis b can be determined via volume conservation ($a = b/\beta$). It is the real root of the cubic equation

$$\begin{aligned} & b^3 + \tfrac{3}{2}(z_0 - z_+)\, b^2 - \tfrac{3}{2} f_0 [\tfrac{1}{5} d (z_0^5 - z_+^5) \\ & - (d z_0^4 + \tfrac{1}{4} c)(z_0^4 - z_+^4) \\ & + (2 d z_0^2 - c z_0 + \tfrac{1}{3})(z_0^3 - z_+^3) \\ & + (d z_0^4 - c z_0^3 + z_0^2)(z_0 - z_+)] - \beta^2 r_0^3 A = 0 . \end{aligned} \tag{3}$$

* The geometrical meaning of the deformation parameter h can be illuminated as follows: At the neck the radius of the compound system is given by the expression $D = a(1-h)^{1/2}$. One can prove that for two separated ions D becomes imaginary ($h > 1$). This was the reason we used h as a deformation parameter rather then D.

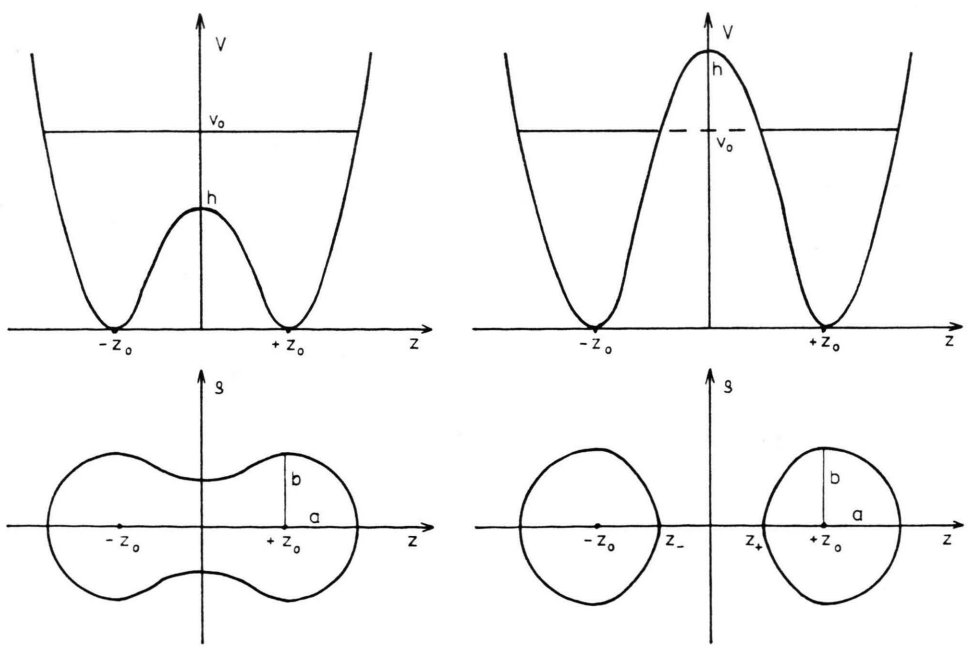

Fig. 1. Typical TCSM potential along the z-axis with the generated nuclear shape. Left side: compound nucleus. Right side: separated ions.

The solution of (3) must be found iteratively because z_+ is an implicit function of b and represents the left edge of the right ion (see Figure 1). z_+ is determined by the solution of the equation

$$d\cdot z^4-(4\,d\,z_0-c)\,z^3+(6\,d\,z_0^2-3\,c\,z_0+1)\,z^2 -(4\,d\,z_0^3-3\,c\,z_0^2+2\,z_0)\,z+d\,z_0^4-c\,z_0^3+z_0^2 -b^2/f_0=0 \tag{4}$$

in the region $0\leqq z<z_0$. For the compound nucleus ($h\leqq 1$) one should set $z_+=0$ in Equation (3).

The parameters c and d are describing the deviation from the ellipsoidal shape. As for $|z|\geqq z_0$ we use a pure ellipsoidal shape, c and d vanish in that (outer) region. In the inner region $|z|<z_0$ they have the values

$$c_r=\frac{1}{z_0}\left(2-\frac{4\,b^2\,h}{f_0\,z_0^2}\right),\quad d_r=\frac{1}{z_0^2}\left(1-\frac{3\,b^2\,h}{f_0\,z_0^2}\right) \tag{5}$$

for the right nucleus and $c_l=-c_r$, $d_l=d_r$ for the left nucleus (reflectional symmetry).

As already shown [9] the shell model potential has additional extrema in the region $|z|<z_0$ if $\varepsilon\equiv b^2\,h/z_0^2<1/6$, $f_0=1$. This determines the range of f_0 as

$$0<f_0\leqq 6\,\varepsilon \tag{6}$$

in this region. The shell corrections depend only negligibly on f_0 while the liquid drop energies show a significant dependence on it. That fact led us to the following equation for calculating f_0 in the inner region

$$\partial E_{LD}/\partial f_0=0\,. \tag{7}$$

We may notice that E_{LD} has only one minimum for $0<f_0\leqq 6\,\varepsilon$. The fact that we are using pure ellipsoidal shapes for $|z|\geqq z_0$ leads to $f_0=1$ in this outer region.

The liquid drop deformation energy E_{LD}^D is defined as usual:

$$E_{LD}^D(\alpha_i)=E_{LD}(\alpha_i)-E_{LD}(0)\,. \tag{8}$$

$E_{LD}(0)$ is the liquid drop energy of two spherical ions at infinite relative distance ($z_0\to\infty$), and $E_{LD}(\alpha_i)$ represents the liquid drop energy for the actual values of the deformation parameter set $\alpha_i=\{z_0,\beta,h\}$. The liquid drop energy E_{LD} itself is defined by:

$$E_{LD}(\alpha_i)=E_{vol}+E_{surf}(\alpha_i)+E_{curv}(\alpha_i) +E_{coul}(\alpha_i)+E_{pair}\,. \tag{9}$$

Because the question whether the curvature energy $E_{curv}(\alpha_i)$ should contribute to E_{LD} or not has so far not been answered unambigously, our calculations are done both ways. The Coulomb energy $E_{coul}(\alpha_i)$ has been calculated numerically according to Lawrence's method [10]. We use two sets of LDM constants: The Lysekil set given by Myers and Swiatecki [11] for E_{LD} without curvature energy contribution, and the set given by Groote and Hilf [12] for E_{LD} containing this contribution. Some calculations have also been made with the Leysin set of LDM constants given by Seeger [13]. All these authors use the constant r_0 from the empirical law $R\approx r_0 A^{1/3}$ also as a LDM constant. Since in their work they investigated only the nuclei with $A\geqq 40$, but we are dealing also with the nuclei with $A<40$, we shall use the experimental values of r_0 in our calculations. Table I shows the r.m.s. radii and the corresponding r_0 for all the nuclei taken into consideration.

2.2. *Liquid Drop Deformation Energies for the Sudden Processes*

We assume that even for extremely sudded processes the nucleons in the nuclei are moving in some average potential and thus there exists some average density during the scattering process. (The effects of the deviation from our assumption are studied in Ref. [14].) That allows us to construct the scattering potential by means of the potential energy surfaces. As during the sudden scattering process the individual properties of the scattered nucleus should be conserved as far as possible, we are going to describe it by $\langle R^2(\alpha_i)\rangle^{1/2}=\langle R^2(z_0=\infty)\rangle^{1/2}$, i.e. the r.m.s. radii should be kept constant throughout the whole process. This causes, of course, a loss of volume and increase of nuclear density in the compound nucleus which yields compression energy. The assumption of uniform density distribution even within the compression zone should be understood as a crude approximation arising from the nondynamical (static) treatment of the compression degree of freedom. The uniform density distribution is given by:

$$\varrho(\alpha_i)=A/v(\alpha_i) \tag{10}$$

where $v(\alpha_i)$ is the nuclear volume for the parameter set α_i. We follow the suggestion of Scheid [15] and set

$$E_{com}(\alpha_i)=\frac{a_{com}}{2\,\varrho_0}\int_{v(\alpha_i)}\mathrm{d}\tau\,[\varrho(\alpha_i)-\varrho_0]^2 \tag{11}$$

Table I. Experimental r.m.s. radii and recalculated $\hbar\omega_\infty$ and r_0 values.

Nucleus	$\langle r^2\rangle^{1/2}$ [fm]	$\hbar\omega_\infty$ [MeV]	r_0 [fm]	Reference
^{12}C	2.42	15.42	1.36	32
^{14}N	2.45	15.31	1.31	33
^{16}O	2.66	13.22	1.36	32
^{20}Ne	2.98	11.678	1.34	34
^{24}Mg	3.01	12.21	1.34	35
^{28}Si	3.086	12.13	1.35	35
^{32}S	3.244	11.73	1.31	35
^{40}Ar	3.47	10.336	1.31	36
^{40}Ca	3.38	10.89	1.28	37
^{42}Ca	3.395	11.054	1.26	38
^{44}Ca	3.442	10.987	1.26	39
^{48}Ca	3.493	11.05	1.241	39
^{46}Ti	3.57	10.41	1.29	40
^{52}Cr	3.66	10.36	1.24	41
^{54}Fe	3.681	10.375	1.257	36
^{56}Fe	3.721	10.272	1.256	36
^{58}Ni	3.725	10.361	1.242	42
^{60}Ni	3.755	10.297	1.238	42
^{62}Ni	3.787	10.217	1.235	42
^{64}Ni	3.826	10.096	1.235	42
^{64}Zn	3.925	9.593	1.267	36
^{66}Zn	3.938	9.606	1.258	36
^{70}Zn	3.966	9.608	1.242	36
^{88}Sr	4.14	9.241	1.202	43
^{90}Zr	4.261	9.171	1.228	36
^{92}Mo	4.310	9.104	1.233	36
^{94}Mo	4.351	9.039	1.235	36
^{96}Mo	4.383	8.976	1.236	36
^{98}Mo	4.416	8.915	1.237	36
^{100}Mo	4.456	8.855	1.239	36
^{116}Sn	4.55	8.427	1.204	44
^{120}Sn	4.64	8.333	1.214	44
^{124}Sn	4.67	8.242	1.209	44
^{142}Nd	4.913	7.878	1.216	45
^{144}Nd	4.944	7.841	1.218	45
^{146}Nd	4.970	7.805	1.219	45
^{148}Nd	5.000	7.770	1.220	45
^{150}Nd	5.048	7.735	1.227	46
^{152}Sm	5.090	7.701	1.231	46
^{162}Dy	5.211	7.539	1.134	46
^{164}Dy	5.218	7.509	1.231	46
^{168}Er	5.260	7.449	1.231	46
^{170}Er	5.264	7.419	1.227	46
^{182}W	5.357	7.252	1.220	46
^{184}W	5.369	7.226	1.219	46
^{186}W	5.373	7.200	1.215	46
^{206}Pb	5.4978	6.959	1.202	47
^{208}Pb	5.49	6.937	1.196	48

where ϱ_0 is the density without compression and a_{com} a model constant which has to be determined. Using Eq. (10) we carry out the trivial integration in Eq. (11) with the result

$$E_{\mathrm{com}}(\alpha_i) = a_{\mathrm{com}} \frac{v_0}{2\,v(\alpha_i)} \left[\frac{v(\alpha_i)}{v_0} - 1\right]^2 A \quad (12)$$

which yields the compression energy E_{com} as a function of the nuclear volume.

During the scattering process the nuclear surface is getting smaller and smaller, and in the limiting case of the two colliding nuclei being compressed to the volume of one of them, it becomes half that of the separated nuclei. At the same time the nuclear surface density increases, and in the limiting case just mentioned there are twice as many nucleons per unit area than before the scattering process. This causes a change in surface tension. Usually one has $E_{\mathrm{surf}} = \sigma S$ with σ the surface tension and S the surface area. Now let the surface tension be density dependent: From Eq. (10) we get

$$E_{\mathrm{surf}}(\alpha_i) = a_s\, g_s(\alpha_i)\,[v(\alpha_i)/v_0]\,A^{2/3}. \quad (13)$$

where a_s is the LDM constant and $g_s(\alpha_i) = S(\alpha_i)/S_0$ is the usual surface ratio. Equation (13) indicates that the surface energy becomes volume dependent as in Ref. [3].

The resulting liquid drop energy for the sudden process is given by

$$E_{\mathrm{LD}}(\alpha_i) = E_v + E_{\mathrm{surf}}(\alpha_i) + E_{\mathrm{curv}}(\alpha_i) + E_{\mathrm{coul}}(\alpha_i) + E_{\mathrm{com}}(\alpha_i) + E_{\mathrm{pair}} \quad (14)$$

where the surface energy E_{surf} is now given by Eq. (13) and the compression energy is given by Equation (11). For the model constant a_{com} of Eq. (11) the value

$$a_{\mathrm{com}} = \tfrac{100}{9}\ \mathrm{MeV}$$

is used, as given in Ref. [3]. This value produces the compression energy of 89 MeV for ^{32}S when compressed to the volume of an ^{16}O nucleus. The total energy difference between the compressed ^{32}S nucleus and two ^{16}O nuclei at infinite relative distance ($z_0 \to \infty$) is about 135 MeV. The preliminary study [14] of the experimental data for this case gives a value of approximately 130 MeV and the calculations within the Thomas-Fermi model yield similar values [16]. If the total energy is calculated by the method of single particle energy summation, this difference turns out to be 270 MeV, which seems too high.

3. Microscopic Part of the Model

3.1. Two-Center Shell Model

The basis of the two-center shell model (TCSM) was given originally by Holzer et alias [17]. Its refined potential can be denoted in cyclindrical coordinates as follows

$$V(\varrho, z) = \tfrac{1}{2} M\,[\omega_\varrho{}^2\,\varrho^2 + \omega^2 z'^2 f_0(1 + c\,z' + d\,z'^2)] \quad (15)$$

where M is the nucleon mass ($M/\hbar^2 = 0.024106$ $\mathrm{MeV}^{-1}\,\mathrm{fm}^{-2}$). The Hamiltonian of the TCSM has the form

$$H = -\hbar^2 \nabla^2/2M + V(\varrho, z) + V_{ls}(\boldsymbol{r}, \boldsymbol{p}, \boldsymbol{s}) + V_{l^2}(l). \tag{16}$$

The spin-orbit potential V_{ls} is of Thomas-type

$$V_{ls} = -\frac{2\hbar\varkappa}{M\omega_\infty}[\nabla V(\varrho, z) \times \boldsymbol{p}]\cdot\boldsymbol{s}. \tag{17}$$

The V_{l^2} potential of the Nilsson model cannot be adapted in an analogous form, because there exists no set of the parameters $\{\varkappa, \mu\}$ that reproduce the observed level sequence [18]. Therefore, we keep the l^2-term in the usual manner

$$V_{l^2} = -\hbar\omega_\infty \varkappa\mu\,[l^2 - \tfrac{1}{2}N(N+3)\,\delta_{if}] \tag{18}$$

where ω_∞ is the asymptotic frequency of the colliding nuclei. Further, δ_{if} means that we are considering only the contribution of the diagonal matrix elements. As usual for the phenomenological shell model, we identify the equipotential surface

$$V_0 = \tfrac{1}{2}M\omega_\infty^2 R_0^2 \tag{19}$$

as a nuclear surface. R_0 is the equivalent uniform radius that can be calculated from r.m.s. radius $\langle R^2\rangle^{1/2}$ by $R_0 = (\frac{5}{3}\langle R^2\rangle)^{1/2}$. We only notice that the spectra show the desirable asymptotic behaviour [17, 19, 20] in both, the sudden and the adiabatic case (Figure 2).

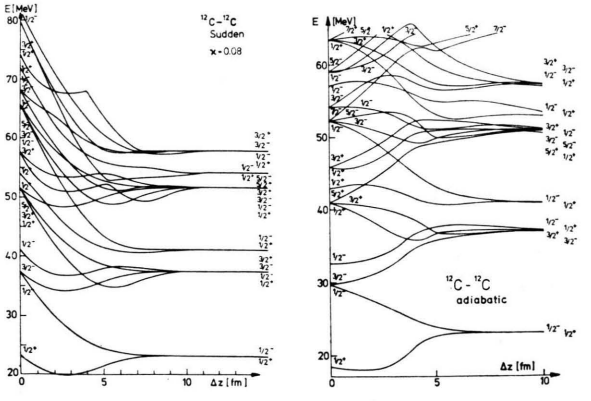

Fig. 2. Single particle levels of Hamiltonian (16) calculated for $^{12}C-^{12}C$ scattering. Each level is labeled by Ω^π. Left side: adiabatic case. Right side: sudden case.

Here we need the energy levels for the calculation of the shell corrections. Therefore, we take only as many basis states as needed for their convergence to 10 keV accuracy. We found that we need, e. g. 150 basis states for the ^{12}C-^{12}C- and 600 basis states for ^{238}U-^{238}U-system.

While for the basis one only has to calculate the quantum numbers as function of the deformation, the definition of some interpolation prescription for the strength coefficients $\varkappa$ and μ of the V_{ls} and V_{l^2} terms as a function of the deformation parameters is needed. The initial values $\varkappa_i$ and μ_i for the independent nuclei and the final values $\varkappa_f$ and μ_f of the compound nucleus are well known [18, 21] (see Figure 3). In the sudden case we want to conserve

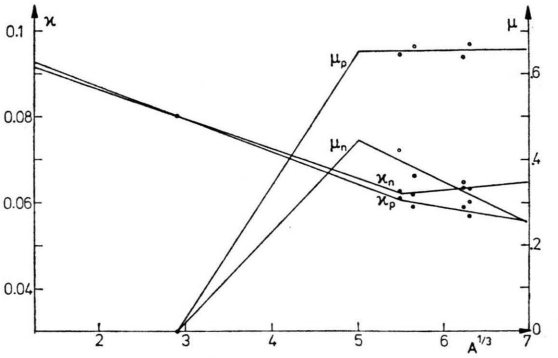

Fig. 3. The values for $\varkappa$ and μ as a function of $A^{1/3}$. Circles and points are the adjustment points of μ an $\varkappa$, respectively, according to Ref. 21.

the individual properties of the colliding nuclei, so we set $\varkappa(\alpha_i) = \varkappa_f = \varkappa_i$ and $\mu(\alpha_i) = \mu_f = \mu_i$ without any interpolation. The adiabatic process is characterized by the volume conservation. The compound nucleus is going to have $\varkappa_f$ and μ_f values that are different from those of the two individual nuclei. In the interpolation prescription we use, $\varkappa$ and μ depend only indirectly on the deformation parameters. We define namely the "intermediate mass number" $A(\alpha_i)$ as follows:

$$A(\alpha_i) = \frac{2A_\infty}{\gamma(\alpha_i)} \tag{20}$$

with $\gamma(\alpha_i) =$

$$= \begin{cases} 1 + h^2 \exp\{-(A_\infty/100\,z)\} & \text{for } h \leqq 1, \\ 2 & \text{for } h > 1, \end{cases}$$

and put $\varkappa(\alpha_i) = \varkappa[A(\alpha_i)]$, $\mu(\alpha_i) = \mu[A(\alpha_i)]$ according to Figure 3. Due to this interpolation the nuclei have their touching point ($h = 1$) at increasing relative distances ($2z_0$) with increasing nucleon number A_∞. Furthermore, in the overlap region the nuclear shapes without or with only a small neck-in are energetically prefered, as expected [8].

4. Construction of the Scattering Potentials

Until now we were interested only in the conservation of the volume of that equipotential surface which corresponds to the nuclear surface ("surface volume conservation"). This kind of conservation gave us the connection between the macroscopic and the microscopic part of the model. For this purpose we have to determine the surface potential V_0 which appears in (19). As we are also dealing with nuclei with $A<40$ for which r_0 is not constant we redetermine the usual

$$\hbar\,\omega_0 = k\,A^{-1/3}\,\mathrm{MeV} \tag{21}$$

prescription with $k=41$ for V_0 (see Ref. [22]). Here we follow Pruess [23] and use the virial law for the oscillator states:

$$\langle t_i\rangle = \langle v_i\rangle = \tfrac{1}{2} M\omega^2 \langle r_i^2\rangle = \tfrac{1}{2}\varepsilon_i\,. \tag{22}$$

Using the definition of the r.m.s. radius $\langle r^2\rangle = 1/A \sum_{i=1}^{A} \langle r_i^2\rangle$ ignoring the spin-orbit and l^2-interactions for the moment and considering (22), we obtain for 1p-shell nuclei

$$\hbar\,\omega = (2.5 - 4/A)\hbar^2/(M\langle r^2\rangle) \tag{23 a}$$

and analogously for the

2s – 1d shell nuclei: (23 b)

$$\hbar\,\omega = (3.5 - 20/A)\hbar^2/(M\langle r^2\rangle)\,,$$

2p – 1f shell nuclei: (23 c)

$$\hbar\,\omega = (4.5 - 60/A)\hbar^2/(M\langle r^2\rangle)\,.$$

In the formulas (23 b, c) the spin-orbit and l^2-interactions are indirectly taken into account, as we replaced the oscillator shells with the states between two magic numbers. One can easily check that (23 c) describes the nuclei with $40<A\leqq 100$. For nuclei in this region, $r_0 = 1.2$ fm can be used and the value $k=41$ as given in Eq. (21), appears already for ^{88}Sr.

These values are very well established in the theory of nuclear fission. The value $r_0 = 1.2$ fm is not changing very much for nuclei with $A \geqq 88$, so that we use the value $k=41$ for all nuclei heavier than ^{88}Sr.

In general the volume is not conserved for every equipotential surface, but this is of negligible influence if the method of shell correction is used to calculate the deformation energy. In practice we use the method of the average volume conservation [24] with the volume conservation function $\lambda(a_i, p)$

$$\lambda(a_i,p) = [b^3 p^{3/2} + \tfrac{3}{2} z_0 b^2 p - f_0\,(\tfrac{3}{10} d z_0^5 - \tfrac{3}{8} c z_0^4 + \tfrac{1}{2} z_0^3)]^{1/3}\,(\beta^2 r_0^3 A)^{-1/3} p^{-1/2} \tag{24 a}$$

for $h \leqq 1$ and

$$\begin{aligned}\lambda(a_i,p) = \{&b^3 p^{3/2} + \tfrac{3}{2}(z_0 - z_+)\,b^2 p - f_0\,[\tfrac{3}{10} d (z_0^5 - z_+^5) \\ &- \tfrac{3}{2}(d z_0 - \tfrac{1}{4} c)(z_0^4 - z_+^4) \\ &+ (3 d z_0^2 - \tfrac{3}{2} c z_0 + \tfrac{1}{2})\cdot(z_0^3 - z_+^3) \\ &- (3 d z_0^3 - \tfrac{9}{4} c z_0^2 + \tfrac{3}{2} z_0)(z_0^2 - z_+^2) \\ &+ \tfrac{3}{2}(d z_0^4 - c z_0^3 + z_0^2)(z_0 - z_+)]\}^{1/3} \\ &\cdot (\beta^2 r_0^3 A)^{-1/3} p^{-1/2}\end{aligned} \tag{24 b}$$

for $h>1$, where $p = V(\varrho, z)/V_0$.

4.2. Shell Correction and Pairing Energy Corrections

For the calculation of Strutinsky's shell correction δU we used Tsang's sixth order polynomial [22] and a smearing width $\Gamma = 1.2\,\hbar\,\omega_0(a_i)$. The insensitivity of δU on Γ for $1\,\hbar\,\omega_0 < \Gamma < 2\,\hbar\,\omega_0$ (Ref. [22]) is confirmed in the case of light and heavy nuclei, but for the super-heavies it is generally not obeyed (see Figure 4). It might be possible that higher

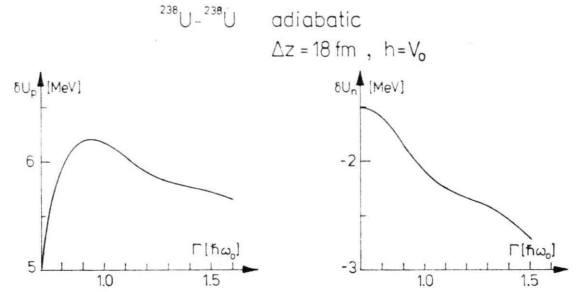

Fig. 4. Non-satisfactory convergence of shell corrections with respect to the choice of smearing factor Γ.

order polynomials than that of Ref. [22] can solve this problem, but this kind of investigations lies beyond the scope of this paper. We used the method described above also for the superheavy compound nuclei in order to give a consistent description for the whole systematics.

To keep the computation time as low as possible, one might try to calculate δU as a function of $\Delta z \equiv 2 z_0$ only- neglecting the h-dependence. Figure 5 shows that the oscillations of δU with $\Delta z =$ const have the same order of magnitude as the oscillations for $h =$ const. This shows that it is not at all allowed to neglect the h-dependence of δU.

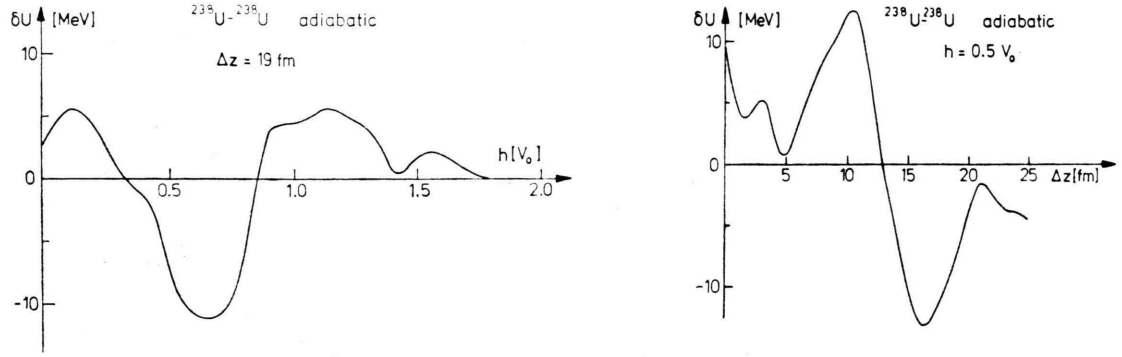

Fig. 5. Shell corrections for $\Delta z = \text{const}$ (left) and $h = \text{const}$ (right) in the adiabatic scattering process $^{238}U - ^{238}U$.

The BCS-theory defines the total energy [23] as (e. g. for protons):

$$E^{p}_{BCS} = 2\sum_{i=1}^{Z} \varepsilon_i v_i^2 - \frac{\Delta}{G} - G\sum_{i=1}^{Z} v_i^4 \qquad (25)$$

where the sums are over the single particle levels i with the energies ε_i occupied by two particles each. Mosel [25] defined the pairing energy corrections as:

$$\Delta P = E^{p}_{BCS} + E^{n}_{BCS} - 2\sum_{i=1}^{Z/2} \varepsilon_i(p) - 2\sum_{i=1}^{N/2} \varepsilon_i(n) \qquad (26)$$

and used the pairing strength G as a free parameter. Nilsson et al. [22] are using the same expression, but they include only 15 proton respectively neutron levels below and above the proton or neutron Fermi-level. Equation (31) includes the assumption that the LDM constants are fitted to the experimental masses without any support from pairing energy, which may not be true, as the LDM constants contain the smooth trend of the pairing energy. This definition may therefore be reasonable for the calculation of the deformation energy by the method of summation of single particle energies. As we are using Strutinsky's method for the shell corrections, we also have to use his method for the pairing energy corrections [5].

4.3. Definition of the Scattering Potential

In analogy to the fission potential the scattering potential is defined by means of the deformation energy $E^D(\alpha_i)$. Within the macroscopic-microscopic method $E^D(\alpha_i)$ is usually given by [5]:

$$E^D(\alpha_i) = E_{LD}(\alpha_i) + \delta U(\alpha_i) + \delta P(\alpha_i) \qquad (27)$$

with $\delta U(\alpha_i) = \delta U_Z(\alpha_i) + \delta U_N(\alpha_i)$ and $\delta P(\alpha_i) = \delta P_Z(\alpha_i) + \delta P_N(\alpha_i)$ as shell and pairing energy correction respectively. The scattering potential can now be defined as:

$$V_{sc}(\alpha_i) = E^D(\alpha_i) - E^D(GS; \Delta z = \infty) \qquad (28)$$

i. e. the numerical value of the scattering potential for the deformation α_i is the difference between the deformation energy of the system at this deformation, $E^D(\alpha_i)$, and the deformation energy of two infinitely separated ($\Delta z = \infty$) nuclei in their ground state $E^D(GS)$.

5. Results and Discussion

From the definition of the scattering potential (28) it is obvious, that the TCSM describes only

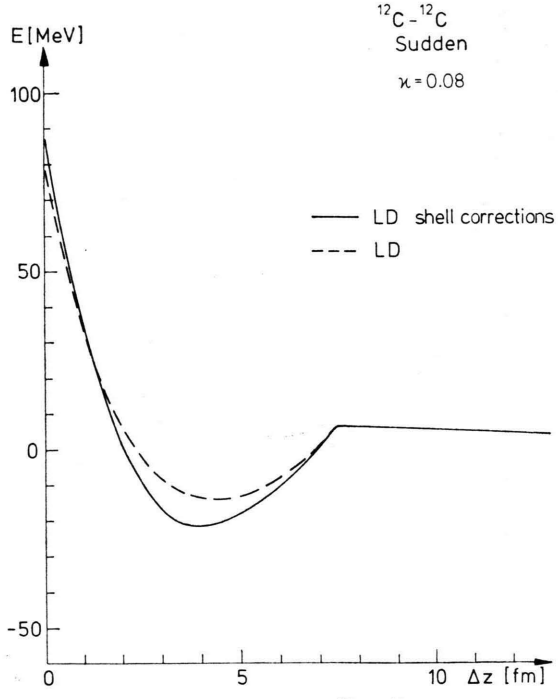

Fig. 6. Potential energy curve for $^{12}C - ^{12}C$ scattering in a sudden approximation. LDM constants are given in Ref. 10.

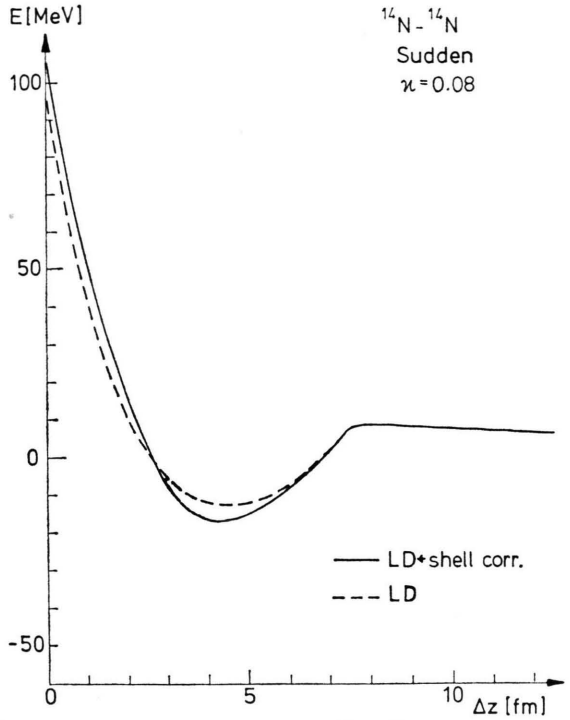

Fig. 7. The same as Fig. 6 for $^{14}N-^{14}N$ scattering. The potential minimum is still lowered by the shell corrections similar to $^{12}C-^{12}C$ potential curve.

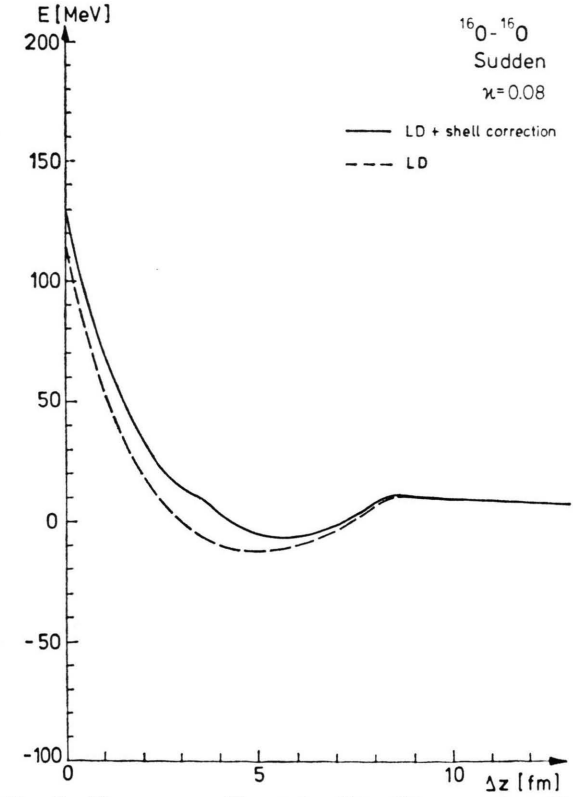

Fig. 8. The same as Fig. 6 for $^{16}O-^{16}O$ scattering. The potential minimum is flattened compared with the pure LD value.

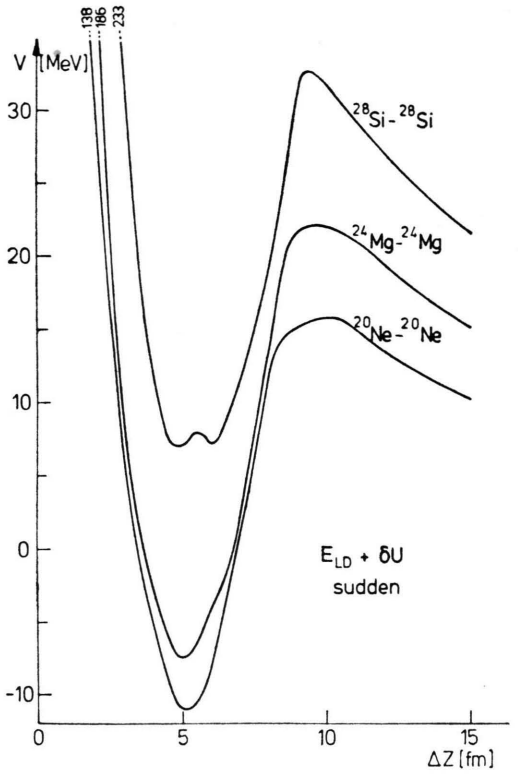

Fig. 9. Potential energy curve for $^{20}Ne-^{20}Ne$, $^{24}Mg-^{24}Mg$ and $^{28}Si-^{28}Si$ scattering in a sudden approximation. The potential minima increase in depth with increasing A.

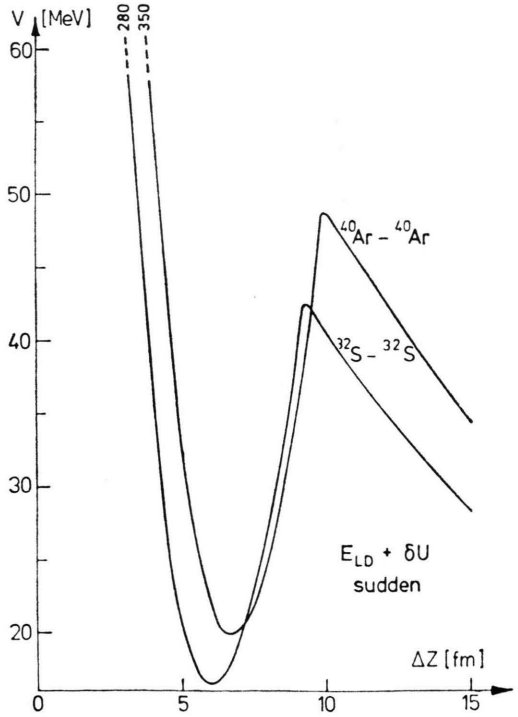

Fig. 10. The same as Fig. 6 for $^{32}S-^{32}S$ and $^{40}Ar-^{40}Ar$ scattering. In the $^{40}Ar-^{40}Ar$ collision the largest potential minimum depth has been achieved.

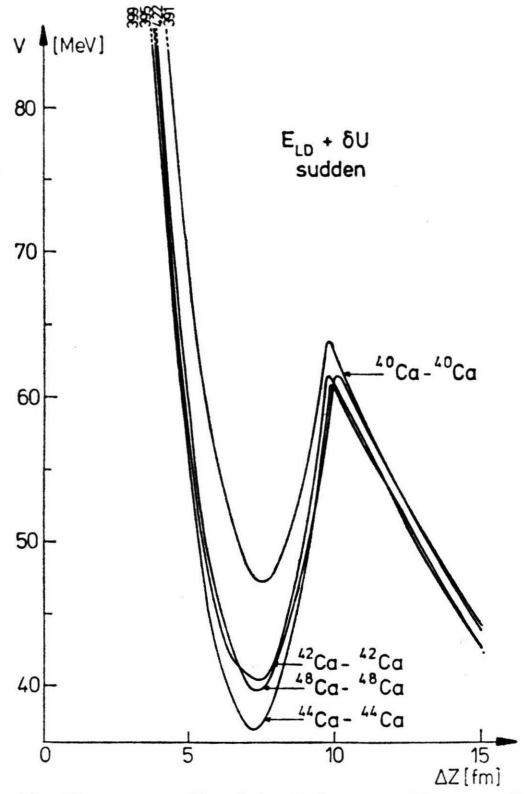

Fig. 11. The same as Fig. 6 for Ca-isotopes. The anomalous behaviour of the ^{48}Ca--^{48}Ca potential is due to the erroneous determination [27] of the r.m.s. radius of ^{48}Ca.

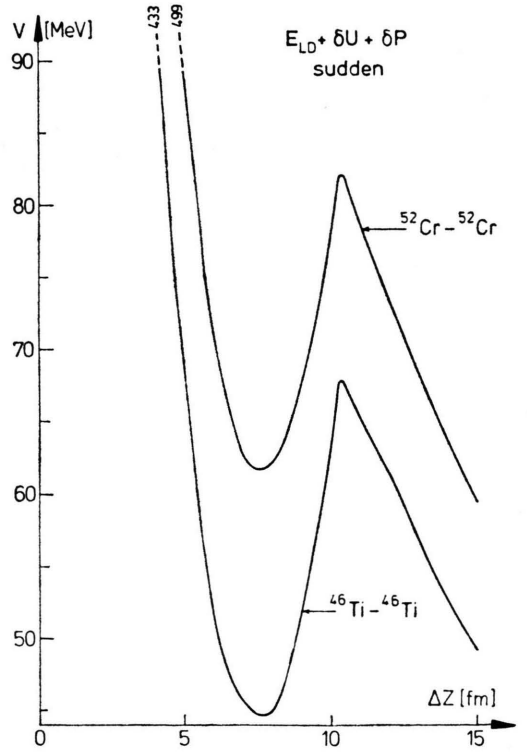

Fig. 12. The same as Fig. 6 for $^{46}Ti-^{46}Ti$ and $^{52}Cr-^{52}Cr$ scattering. The depth of the potential minimum decreases with the increasing A.

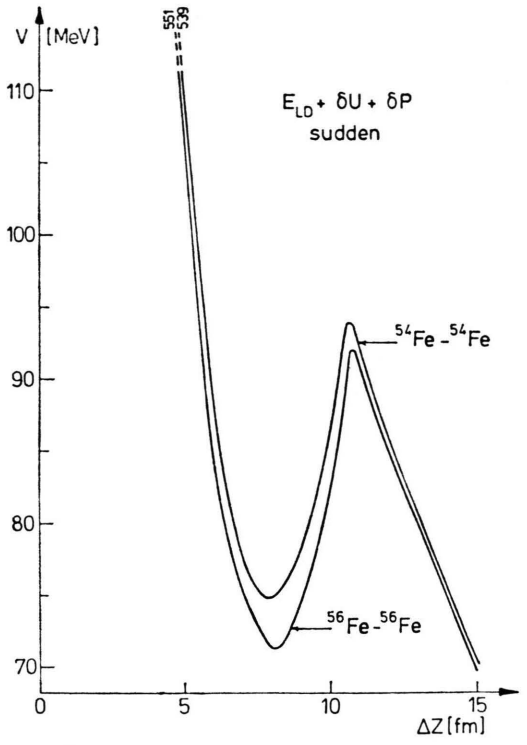

Fig. 13. The same as Fig. 6 for Fe-isotopes. In the isotopic chain the potential minimum depth is increasing with increasing A.

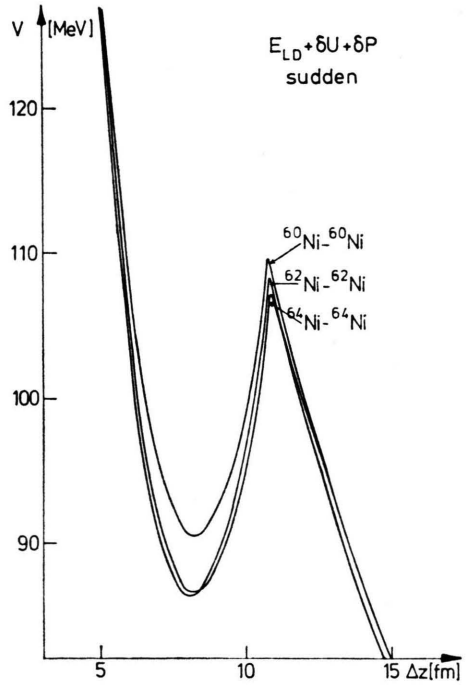

Fig. 14. The same as Fig. 6 for Ni-isotopes. For the isotopic chain there is a shift of the potential minimum toward smaller separations Δz for increasing A.

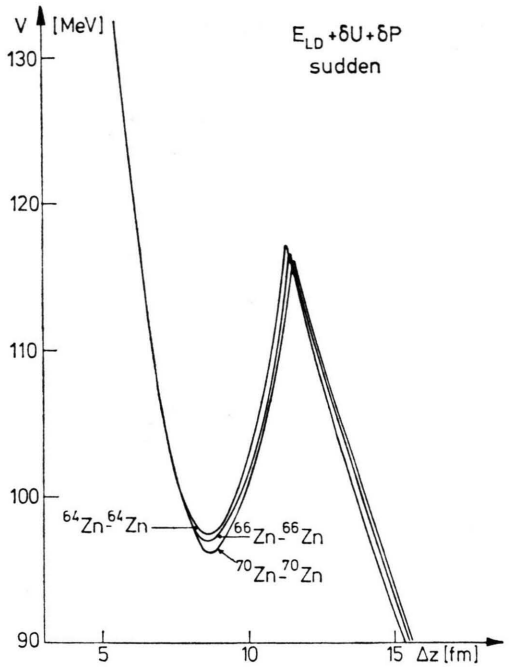

Fig. 15. The same as Fig. 6 for Zn-isotopes. The Coulomb barrier is shifted toward larger separations Δz with increasing A.

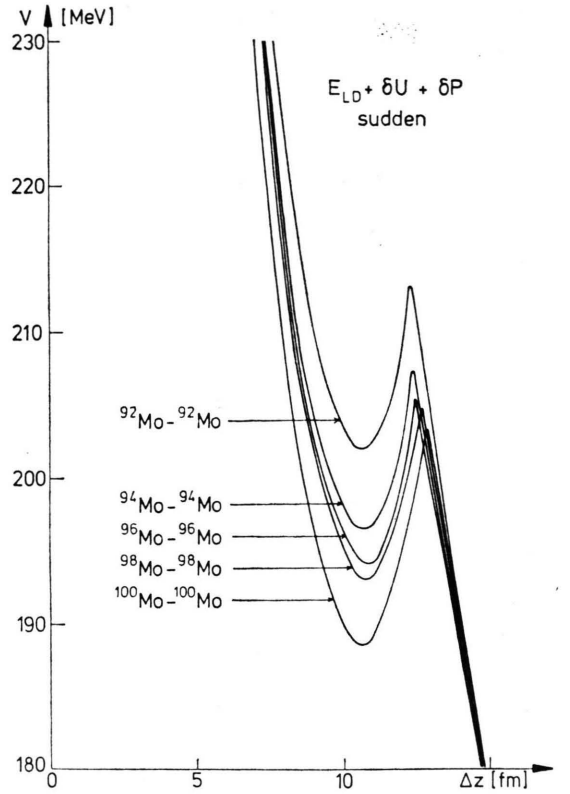

Fig. 17. The same as Fig. 6 for Mo-isotopes. The positions of the Coulomb barriers and potential minima are shifted to the larger separations Δz with increasing A. The depths of the potential minima increase with increasing A.

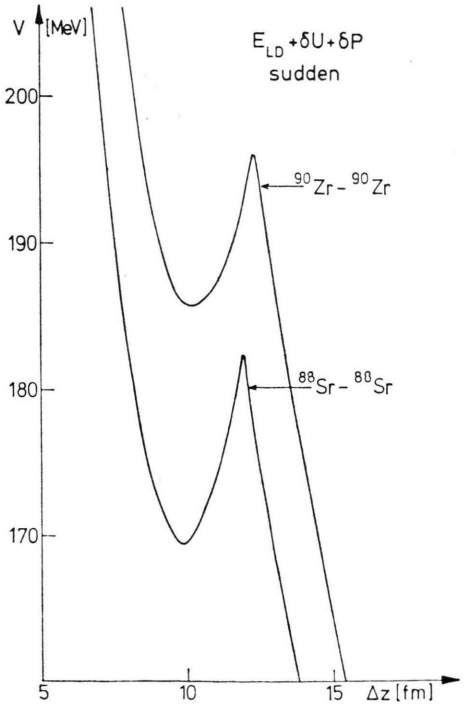

Fig. 16. The same as Fig. 6 for $^{88}Sr-^{88}Sr$ and $^{90}Zr-^{90}Zr$ scattering. The potential minimum depth of the $^{90}Zr-^{90}Zr$ scattering potential is smaller then $^{88}Sr-^{88}Sr$ potential minimum depth.

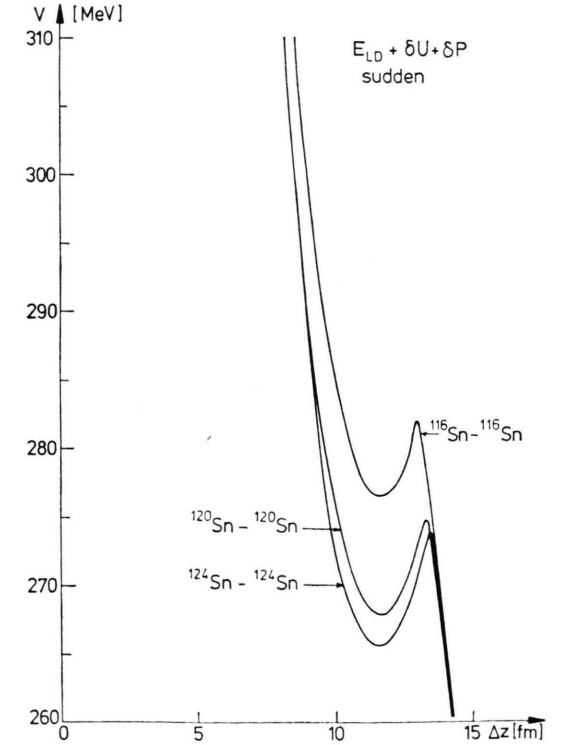

Fig. 18. The same as Fig. 6 for Sn-isotopes. The depths of the potential minima are already small compared with the potentials of the lighter nuclei (Fig. 6—Figure 17).

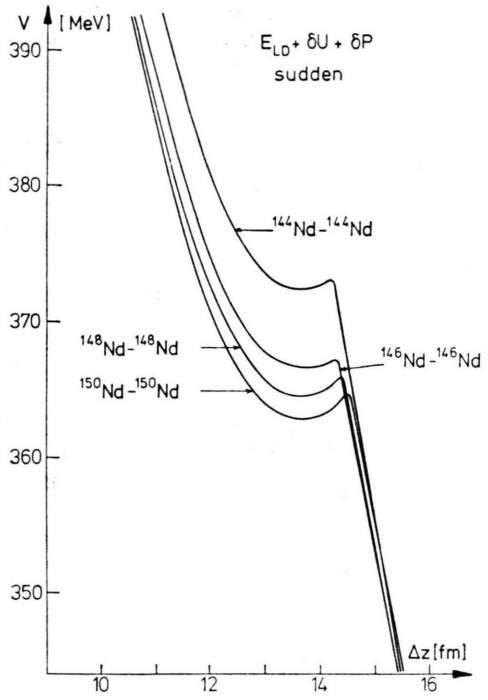

Fig. 19. The same as Fig. 6 for Nd-isotopes. The potential minima are so flat that no molecular states (resonances) can be expected for the collisions of identical Nd-nuclei.

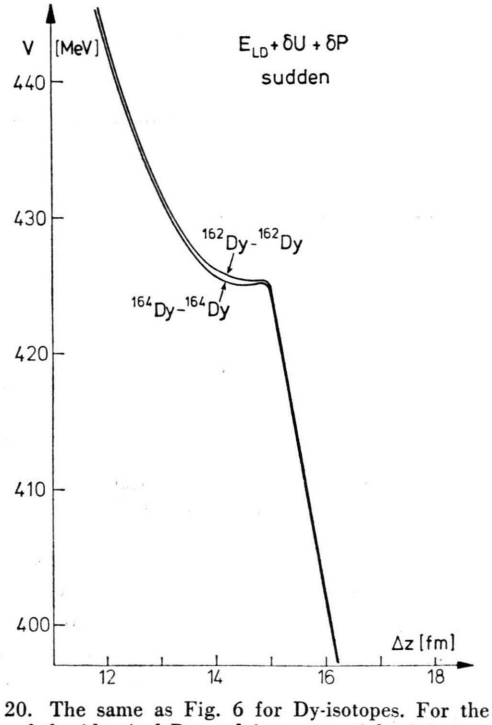

Fig. 20. The same as Fig. 6 for Dy-isotopes. For the collision of the identical Dy-nuclei no potential minima can be observed.

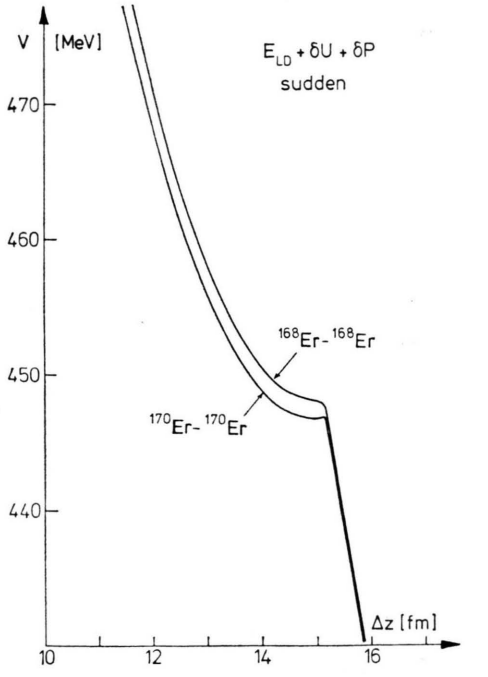

Fig. 21. The same as Fig. 6 for Er-isotopes. There is no potential minimum for the scattering of identical Er-nuclei. The Coulomb barrier is still lowered and shifted towards larger separations Δz for increasing A.

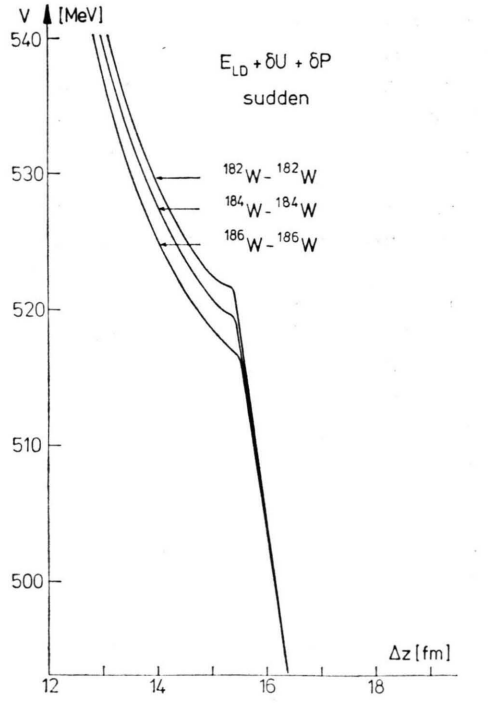

Fig. 22. The same as Fig. 6 for W-isotopes. W-nuclei produce no potential minima during the scattering.

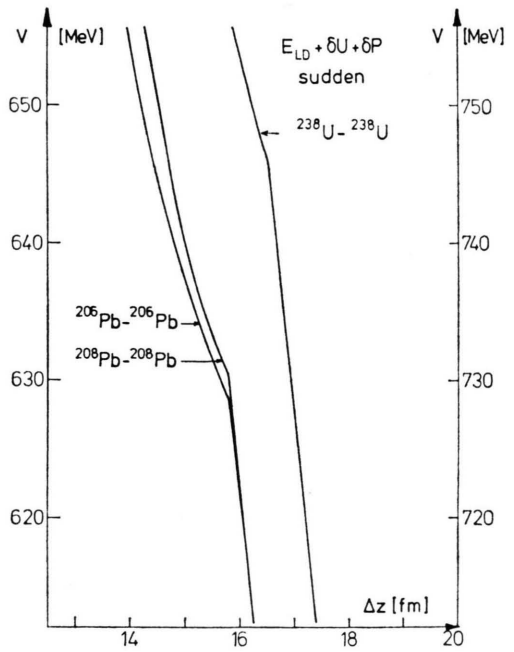

Fig. 23. The same as Fig. 6 for Pb-isotopes and for $^{238}U-^{238}U$ scattering. Left energy scale corresponds to the Pb-isotopes, the right side scale to $^{238}U-^{238}U$. The Coulomb barrier is indicated only by the change in the potential slope.

the static effects of the heavy ion scattering process. For the dynamic aspects of this problem we refer to some interesting statements in References [14, 26].

We now discuss systematically the results for the heavy ion scattering potentials in the sudden case. The Figs. 6 – 23 show several such potential curves especially in the vicinity of the Coulomb barrier. In the numerical calculations steps of 0.2 fm for Δz have been used. All the potentials have been normalized to zero for infinite separation. For this series of the potentials we used the LDM parameters as given in Ref. [11]. The oscillator frequencies have been recalculated from the r.m.s. radii by the prescription described above.

The expected results are firstly: The shift of the Coulomb-barrier towards higher values of Δz for increasing nuclear mass A. One can see that shift e. g. for the Mo-isotopes in Fig. 17 and for the Ca-isotopes in Figure 11. The anomalous behaviour of the ^{48}Ca-^{48}Ca scattering potential may be explained by the error in the determination of the r.m.s. radius, as the neutron form factor has not be taken into account properly [27]. Secondly, one can see that the potential minima, responsible for the formation of the nuclear molecules, deepen with increasing A, obtaining their largest depth for the ^{40}Ar-^{40}Ar scattering potential (ca. 30 MeV), and are flattening for nuclei heavier than ^{40}Ar. Also for the isotopic chains the potential depths vary as expected: The heaviest isotopes have the deepest minima due to the Coulomb energy. This minimum disappears in the rare earth region: The Nd-isotopes (Fig. 19) have very flat minima, so that one can expect no molecular states for these potentials. For the heavier nuclei the molecular minima disappear completely: the Couomb barrier vanishs at all, and only the change in the potential slope indicates, in Fig. 23, the touching point of nuclei. The absence of the potential minima has no influence on the main resonance structure of the excitation function as already seen for ^{16}O-^{16}O elastic scattering at high c. m. energies [28].

The influence of the shell corrections can be studied in Figures 24 – 26. For ^{12}C-^{12}C and

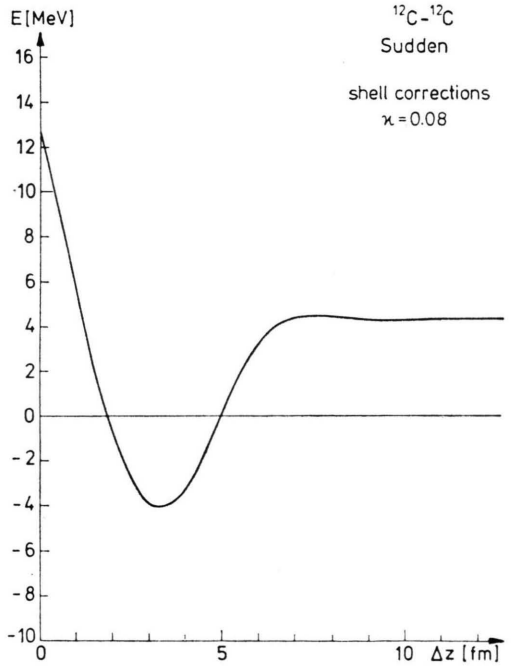

Fig. 24. Shell corrections (absolute value) for $^{12}C-^{12}C$ scattering in the sudden approximation.

^{14}N-^{14}N scattering the shell corrections lower the potential minimum while for ^{16}O-^{16}O scattering we notice the flattening of it. It is evident that the shell corrections change systematically and, starting with positive values for the ^{12}C-^{12}C scattering potential, they fall towards negative values for the ^{16}O-^{16}O system.

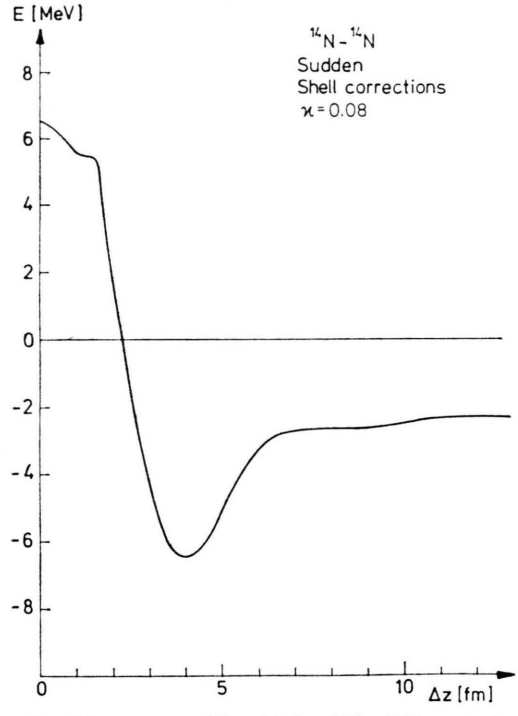

Fig. 25. The same as Fig. 24 for $^{14}N-^{14}N$ scattering. In the region between 2 fm and 6 fm the shell correction lowers the potential energy curve (compare with Figure 7).

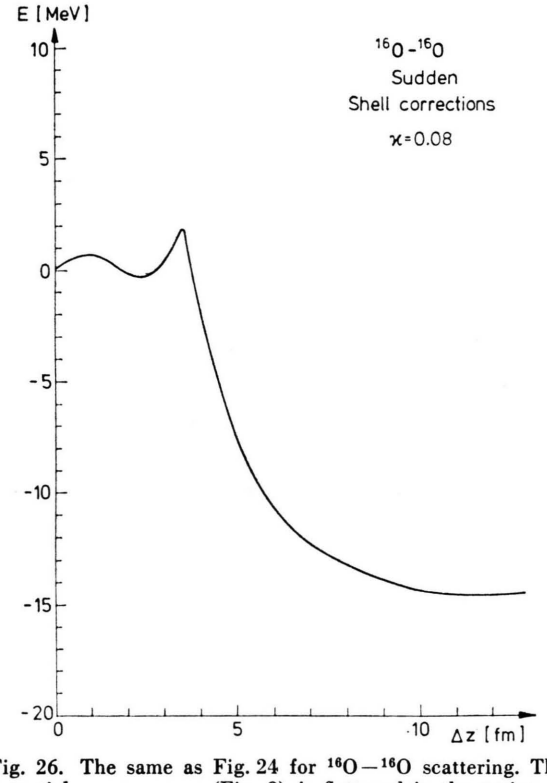

Fig. 26. The same as Fig. 24 for $^{16}O-^{16}O$ scattering. The potential energy curve (Fig. 8) is flattened in the region of the potential minimum.

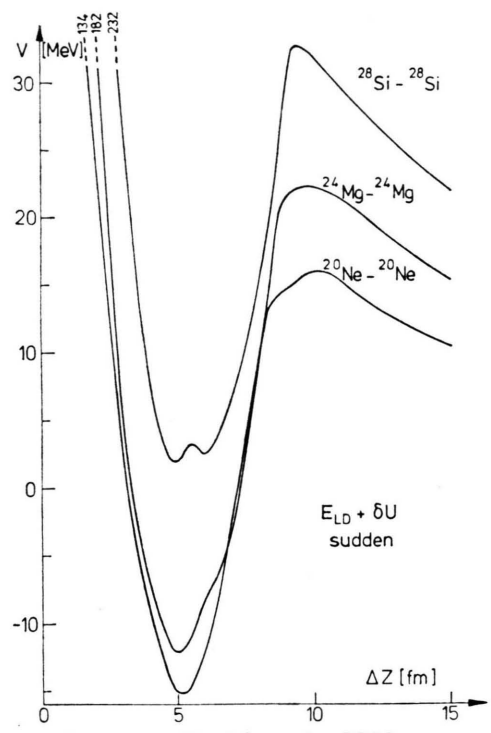

Fig. 27. The same as Fig. 9 but using LDM constants from Ref. 11. The LD energy contains a curvature energy term.

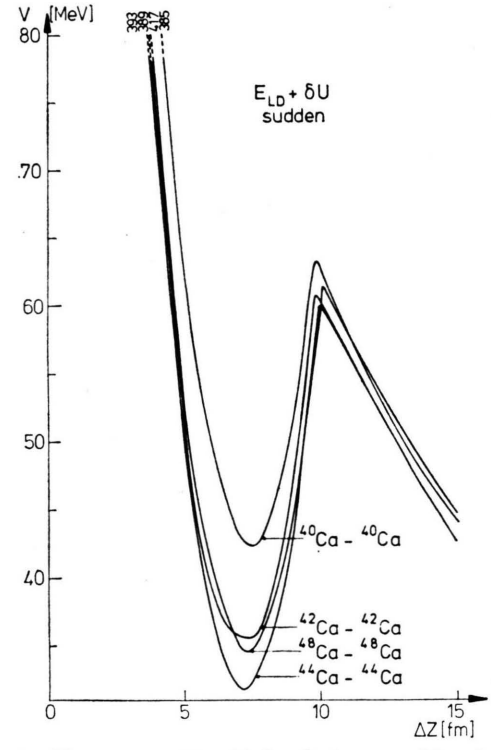

Fig. 28. The same as Fig. 24 for Ca-isotopes. The absolute heights of the Coulomb barrier and potential minimum are decreased compared with Fig. 11 (no curvature energy term). The relative depths of the potential minima are larger than in Figure 11.

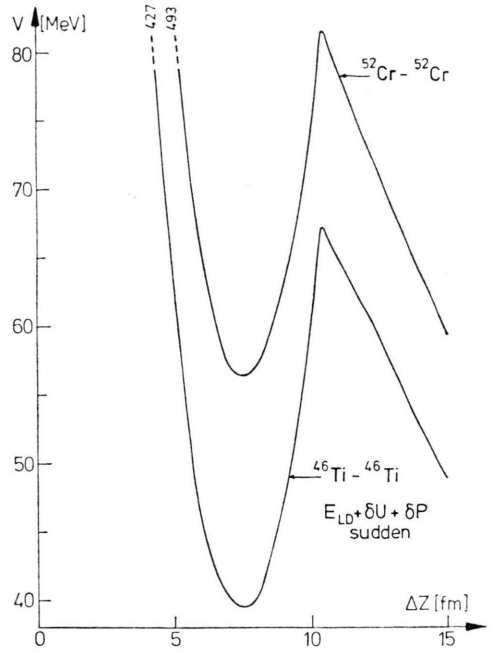

Fig. 29. The same as Fig. 27 for ^{46}Ti—^{46}Ti and ^{52}Cr—^{52}Cr scattering. The comparison with Fig. 12 shows a decrease of the absolute height of Coulomb barrier and potential minimum as well as an enlargement of the relative depth of the potential minimum due to the curvature energy.

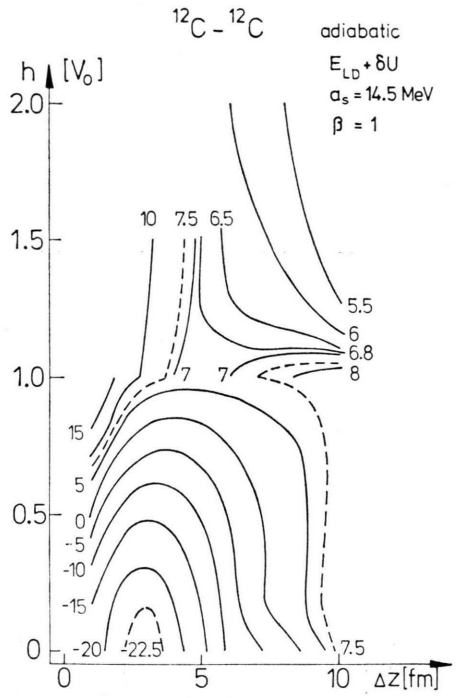

Fig. 30. Potential energy surface for ^{12}C—^{12}C collision in adiabatic approximation. The surface energy constant a_s has been changed to -14.5 MeV. The distance between the contour lines is given in MeV units. The compound nucleus ^{24}Mg has a highly deformed ground state ($\Delta z = 3$ fm, $h = 0$).

The Figs. 27 – 29 show the scattering potentials including the curvature term in the LD part of the model. The comparison with the Figs. 9, 11, 12 shows, that the curvature term tends to increase the relative depth of the potential minima. The Coulomb barriers have not changed their position, but the whole potentials have been reduced.

The main effect is of course the change in the relative depth of the minima. This can be explained by the fact that with increasing overlap of the nuclei during the scattering process, the curvature of the compound system decreases which leads to the smaller absolute value of the curvature energy.

For studying the scattering potentials in the adiabatic approximation, the total PES need to be known. The dynamics of the scattering process develops within these PES and can be studied after the kinetic part of the scattering Hamiltonian is calculated. We restrict ourselves here to the PES only, which are presented in the Figures 30 – 35.

a) ^{12}C-^{12}C (Fig. 30)

For this PES we had to change the surface constant of the LDM, to achieve the proper binding energy difference between the ^{24}Mg nucleus and two ^{12}C nuclei, the value being $a_s = -14.5$ MeV. The main feature of this PES is, that one may expect the Coulomb barrier to be situated somewhere at $\Delta z = 5$ fm. This means, if we compare it with the sudden approximation where the Coulomb barrier appears at $\Delta z = 7.4$ fm, that both ^{12}C nuclei deform very much before touching. The PES minimum of the ^{24}Mg ground state is situated at the deformation coordinates $\Delta z \approx 3$ fm, $h = 0$. This is a reasonable result as there exists the estimate $\Delta z = 3.16$ fm for the ^{24}Mg ground state [15] based on the recalculation of the ^{24}Mg-quadrupole moment in terms of TCSM deformation coordinates. The height of the Coulomb barrier is also satisfactorily reproduced compared wiht the experimental results [29].

b) ^{16}O-^{16}O (Fig. 31)

Here one finds two minima in the PES. The spherical minimum is deeper (-13.5 MeV) while the second minimum at the large prolate deformation $\Delta z = 5$ fm, $h = 0.05$ is only -9.8 MeV deep.

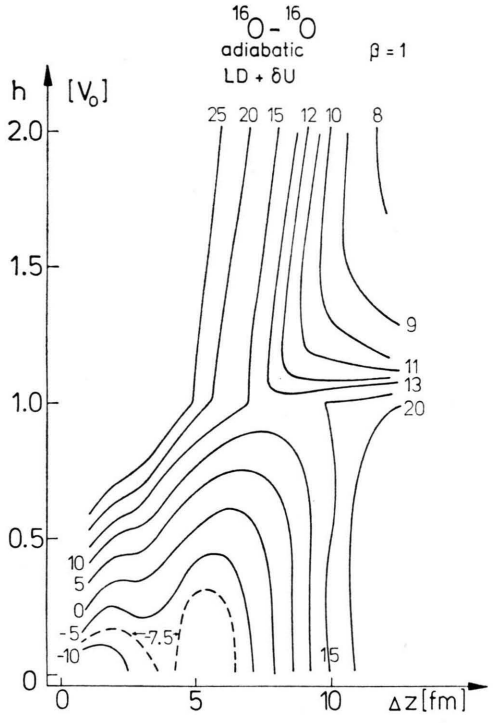

Fig. 31. The same as Fig. 30 for $^{16}O-^{16}O$ scattering but using the original values [10] for the LDM constants. At $\Delta z=0$ fm, $h=0$ and $\Delta z=5$ fm, $h=0.05$ there occur two minima which contribute to the ground state configuration of the compound nucleus ^{32}S.

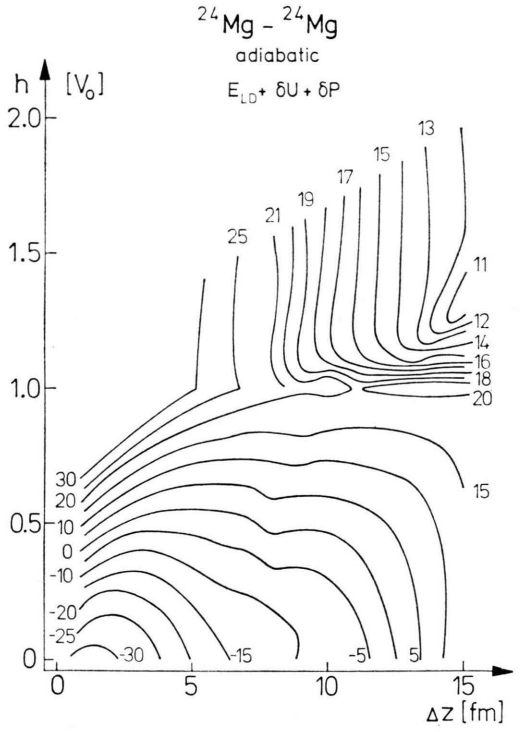

Fig. 32. The same as Fig. 31 for $^{24}Mg-^{24}Mg$ scattering. At the touching line ($h=1$) two saddles appear (at $\Delta z=$ 11 fm and $\Delta z=9$ fm, respectively) which lead to two collision paths through this PES. The compound nucleus ^{48}Cr has a deformed ground state ($\Delta z=1$ fm, $h=0$).

This second minimum has also been predicted by Hartree-Fock type calculations [30]. The Coulomb barrier is situated at $\Delta z=8.1$ fm similar to the Coulomb barrier in the sudden approximation. The height of 13 MeV seems to be about 2 MeV too high if compared with experiment [29].

c) ^{24}Mg-^{24}Mg (Fig. 32)

In this case there exist two saddles at the touching line $h=1$. The saddle at $\Delta z=11$ fm has the height of 19.8 MeV while the height of the other one at $\Delta z=9$ fm is 20.3 MeV. In between one finds a maximum of 21.7 MeV. Obviously there exist two paths through this PES and one can expect that these two possible scattering processes interfere. Only dynamic calculations can clarify this point. It should be interesting indeed to study the excitation function in this energy region. From this PES the deformed ground state of ^{48}Cr ($\Delta z=1$ fm, $h=0$) can be predicted.

d) ^{28}Si-^{28}Si (Fig. 33)

Between $\Delta z=0$ and $\Delta z=3$ fm, $h=0$, one can find a valley of uniform depth (-27 MeV) which describes the quite complicated ground state of ^{56}Ni. A second flat minimum is situated at very large prolate deformation $\Delta z=12$ fm. It is obvious that this minimum with the depth of -3.7 MeV has no influence on the ground state shape, but it is possible that it has some influence on the scattering path.

The Coulomb barrier, which can be found at $\Delta z=14$ fm, is somewhat underestimated [31]. The appearance of the Coulomb barrier at such large prolate deformations is due to the softness of the ^{28}Si nuclei which can be easily deformed even before touching.

e) ^{32}S-^{32}S (Fig. 34)

The structure of this PES is similar to the one of ^{28}Si-^{28}Si. The shell correction effect at large prolate

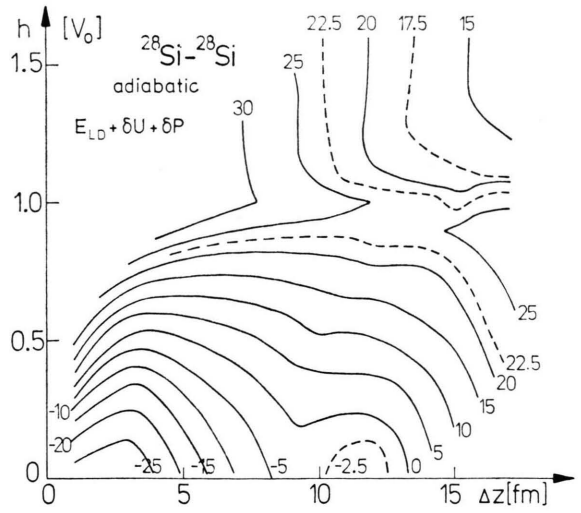

Fig. 33. The same as Fig. 31 for $^{28}Si-^{28}Si$ scattering. Two minima can be observed: at $\Delta z=0-3$ fm, $h=0$ and $\Delta z=12$ fm, $h=0$. The second minimum has no influence on the ground state of the compound nucleus ^{56}Ni.

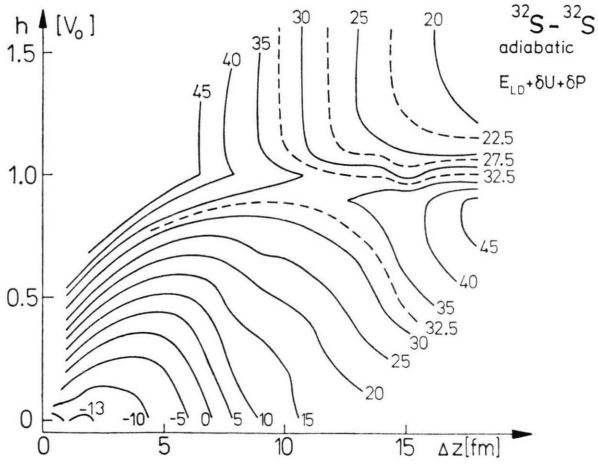

Fig. 34. The same as Fig. 31 for $^{32}S-^{32}S$ scattering. The compound system shows two minima, at $\Delta z=0$ fm, $h=0$ and $\Delta z=2$ fm, $h=0$ respectively, separated by a low barrier. This configuration describes an anharmonic vibrational nucleus.

deformation is still present ($\Delta z=15$ fm). The Coulomb barrier can be found at $\Delta z=11.5$ fm which indicates that the ^{32}S nucleus is more difficult to deform than the ^{28}Si nucleus. The compound system has two minima: a spherical one with -14.3 MeV depth and a deformed one at $\Delta z=2$ fm, $h=0$ with -13.7 MeV depth. This configuration describes an anharmonic vibrational nucleus which we also expect for the ^{32}S nucleus itself.

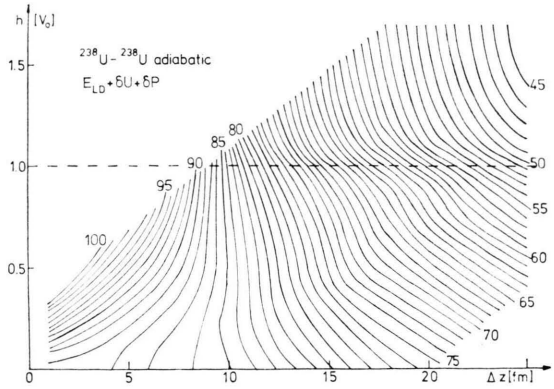

Fig. 35. The same as Fig. 31 for $^{238}U-^{238}U$ scattering. No minimum can be observed in this PES. The contour lines have 10 MeV equidistance and their value has to be multiplied by a factor 10.

f) ^{238}U-^{238}U (Fig. 35)

The investigation of this superheavy system shows that there exists no minimum for the compound system. The compound system, even reached, should immediately undergo fission, at least with respect to symmetric fission. Otherwise it is possible that the asymmetry effects may produce a quasi stable state during rearrangement from the symmetric to the asymmetric geometrical shape. The electronic binding energy may also cause the same effect. An investigation on that point is in progress.

The Coulomb barrier can be determined by a change in the potential gradient somewhere between $\Delta z=19$ and $\Delta z=21$ fm.

All PES are calculated using steps of 1 fm in Δz-direction and 0.1 in h-direction. The computation time was between 0.5 and 2 min/deformation point on the UNIVAC 1108, depending on the number of the basis set functions used.

6. Concluding Remarks

In this article we have calculated real scattering potentials using the Two Center Shell Model (TCSM). In the macroscopic part of the model we improved the nuclear shape parametrization and connected it successfully with an improved microscopic part. That enabled us to describe most of the possible nuclear shapes that may occur during the scattering process, starting with the separated ions up to the compound nucleus. This description has been used for two types of possible scattering processes, the adiabatic and the sudden one.

We described the static effects of nuclear collision. It is natural to proceed to dynamic calculations containing besides the static potentials also the dynamic masses. It should also be noted that our results are in good agreement with the scattering potentials calculated within the framework of the Hartree-Fock model [30] in those cases (^{12}C-^{12}C and ^{16}O-^{16}O) which allow the comparison. *Our main result is that nuclear molecular states (resonances) in nucleus-nucleus collisions should disappear for system around Nd or Dy.* With the new heavy ion accelerators this should be subject to experimental tests.

Acknowledgements

We thank Prof. W. Scheid, Dr. K. Albrecht, Dr. J. Maruhn, and Dr. D. Scharnweber for fruitful discussions and their cooperation in treating numerical problems. We are indebted to Mrs. B. Utschig for drawing the figures for us so nicely. The numerical calculations were carried out at the Hochschul-Rechenzentrum der Universität Frankfurt am Main.

[1] see e.g. Proc. Int. Conf. on Nuclear Reactions Induced by Heavy Ions at Heidelberg (North-Holland, Amsterdam 1970), or Heavy Ion Scattering, Proc. of Symposium held at Argonne Nat. Lab. 1971, Report ANL-7837.
[2] W. Scheid, R. Ligensa, and W. Greiner, Phys. Rev. Lett. **21**, 1479 [1968]; R. A. Brueckner, J. R. Buchler, and M. M. Kelly, Phys. Rev. **173**, 944 [1968].
[3] W. Scheid and W. Greiner, Z. Phys. **226**, 364 [1969].
[4] K. Pruess and W. Greiner, Phys. Lett. **33 B**, 197 [1970]; K. Pruess, Ph. D. Thesis, Inst. für Theoretische Physik der Universität Frankfurt am Main, 1972, unpublished.
[5] see M. Brack, J. Damgaard, A. S. Jensen, H. C. Pauli, V. M. Strutinsky, and C. Y. Wong, Rev. Mod. Phys. **44**, 320 [1972], and references therein.
[6] L. Wilets, A. Goldberg, and F. H. Lewis, Jr., Phys. Rev. **C 2**, 1576 [1970].
[7] U. Mosel, T. D. Thomas, and P. Riesenfeldt, Phys. Lett. **33 B**, 565 [1970].
[8] A. J. Sierk and J. R. Nix, Los Alamos Report, LA-UR-73-981 (1973).
[9] J. Maruhn, Diplomarbeit, Inst. für Theor. Physik der Universität Frankfurt (Main) 1971.
[10] J. N. P. Lawrence, Los Alamos Report, LA-3774 (1967); K. Albrecht, Nucl. Phys. **A 207**, 225 [1973].
[11] W. D. Myers and W. J. Swiatecki, Ark. Fys. **36**, 343 [1966].
[12] H. v. Groote and E. Hilf, Nucl. Phys. **A 129**, 513 [1969].
[13] D. A. Seeger, Proc. Int. Conf. on Properties of Nuclei far from the Region of Beta-Stability, Leysin, 1970, Geneva Report CERN 70-30 (1970), p. 217.
[14] S. Liran, H.-J. Scheefer, W. Scheid, and W. Greiner, Nucl. Phys. **A 248**, 191 [1975].
[15] W. Scheid, Habilitationsschrift, Inst. für Theor. Physik der Universität Frankfurt (Main) 1970.
[16] V. R. Pandharipande, Phys. Lett. **31 B**, 635 [1970].
[17] P. Holzer, U. Mosel, and W. Greiner, Nucl. Phys. **A 128**, 241 [1969].
[18] C. Gustafsson in Ref. 12, p. 654.
[19] J. Maruhn and W. Greiner, Z. Phys. **251**, 431 [1972].
[20] D. Scharnweber, U. Mosel, and W. Greiner, Phys. Rev. Lett. **24**, 601 [1970].
[21] I. Ragnarsson in Ref. 12, p. 847.
[22] S. G. Nilsson, C. F. Tsang, A. Sobiezewski, Z. Szymanski, S. Wyzech, C. Gustafsson, I.-L. Lamm, P. Möller, and B. Nilsson, Nucl. Phys. **A 131**, 1 [1969].
[23] G. Baumgärtner and W. Schuck, Kernmodelle, BI Mannheim 1968, p. 153.
[24] K. Albrecht, D. Scharnweber, W. Greiner, and U. Mosel, Phys. Lett. **32 B**, 229 [1970].
[25] U. Mosel, Phys. Rev. **C 6**, 971 [1972].
[26] H.-J. Fink, W. Greiner, R. K. Gupta, S. Liran, J. Maruhn, W. Scheid, and O. Zohni, Theory of Fragmentation in Nuclear Fission and Nucleus-Nucleus Collision, Proc. Int. Conf. on Reactions between Complex Nuclei, Nashville, June 1974 (North-Holland Publ. Comp.); J. R. Nix and A. J. Sierk, paper presented at Nobel Symposium on Superheavy Elements, Ronneby, Sweden, June 1974.
[27] D. A. Bromley, private communications.
[28] M. L. Halbert et al., Bull. Amer. Phys. Soc. **18**, 1387 [1973], and Phys. Lett. **51 B**, 341 [1974].
[29] D. A. Bromley, in Ref. 3, p. 27.
[30] G. Reidemeister, Nucl. Phys. **A 197**, 631 [1972], and D. Kolb, Contributions to the Int. Conf. on the Reactions Between Complex Nuclei, Nashville 1974.
[31] A. J. Ferguson et al., Report ANL-7837, p. 187.
[32] T. W. Donelly and G. E. Walker, Phys. Rev. Lett. **22**, 1121 [1969].
[33] U. Meyer-Berkhout et al., Ann. Phys. **8**, 119 [1959].
[34] P. Brix, quoted by G. Ripka, in Nuclear Structure Studies using Electron Scattering and Photo-Reaction, ed. K. Shoda and H. Ui, Tokohu University, Sendai 1972.
[35] G. Backenstoss et al., Phys. Lett. **25 B**, 547 [1967].
[36] H. Ehrenberg, Contributions to the Proc. of the Int. Conf. on Nuclear Structure Studies using Electron Scattering and Photoreactions, Sendai, Japan, 1972, p. 85.
[37] R. Shaw et al., Proc. Phys. Soc. London **86**, 513 [1965].
[38] D. F. Jackson, Phys. Lett. **32 B**, 233 [1970].
[39] L. R. Elton, Phys. Rev. **158**, 970 [1967].
[40] H. Theissen et al., Phys. Lett. **22**, 623 [1966].
[41] J. B. Bellicard et al., Nucl. Phys. **60**, 319 [1964].
[42] J. R. Ficenec et al., Phys. Lett. **32 B**, 460 [1970].
[43] R. H. Helm, Phys. Rev. **104**, 1466 [1956].
[44] P. Bareau and J. B. Bellicard, Phys. Lett. **25 B**, 470 [1967].
[45] J. H. Heisenberg et al., Nucl. Phys. **A 164**, 340 [1971].
[46] D. Hitlin et al., Phys. Rev. **C 1**, 1184 [1970].
[47] H. L. Anderson et al., Phys. Rev. Lett. **22**, 221 [1969].
[48] Landolt-Börnstein, Zahlenwerte und Funktionen aus Naturwissenschaft und Technik, Vol. I/2, Springer-Verlag. Berlin 1967.